scientific reports

OPEN

Enhanced antimicrobial efficacy and biocompatibility of albumin nanoparticles loaded with *Mentha* extract against methicillin resistant *Staphylococcus aureus*

Hadi Zare-Zardini [1]✉, Ameneh Alizadeh [2]✉, Elham Saberian [3], Andrej Jenča [3], Andrej Jenca [3]✉, Adriána Petrášová [3], Janka Jenčová [3], Seyede Tahmine Hasani[4], Mohammad Amin Heidari[5] & Nafiseh Sahraei[6]

In an effort to combat methicillin-resistant *Staphylococcus aureus* (MRSA), this study investigates the potential of *mentha*-loaded albumin nanoparticles (MLAN) as a novel antimicrobial agent. MLAN was synthesized by a desolvation method in which the *mentha* extract was encapsulated in albumin nanoparticles to increase stability and reduce toxicity. Characterization of the nanoparticles by transmission electron microscopy (TEM), Fourier transform infrared spectroscopy (FTIR), dynamic light scattering (DLS), and X-ray Diffraction (XRD) confirmed their spherical morphology, a size range of 100–200 nm and uniform distribution. The encapsulation efficiency (EE%) and loading capacity (LC%) of MLAN were determined to be 80% and 72.73%, respectively, indicating a high effectiveness of the encapsulation process. Evaluation of cytotoxicity using the MTT assay revealed that MLAN exhibited significantly higher biocompatibility compared to aqueous Mentha extract and maintained cell viability at $85.1 \pm 3.5\%$ at the highest concentration tested (250 µg/mL). Antimicrobial evaluations against MRSA showed that MLAN had larger zones of inhibition and lower minimum inhibitory concentration (MIC) and minimum bactericidal concentration (MBC) values (0.39 mg/mL and 0.78 mg/mL, respectively) compared to the aqueous extract (MIC: 0.78 mg/mL, MBC: 1.56 mg/mL). In addition, real-time PCR showed that MLAN significantly downregulated the expression of key virulence genes (icaA, icaD and ebps) in MRSA, indicating a potential reduction in bacterial virulence. These results suggest that MLAN could be a promising alternative to conventional antibiotics with improved antimicrobial efficacy and reduced cytotoxicity. The study underlines the potential of combining plant extracts with nanotechnology for the development of new therapeutic approaches against antibiotic-resistant pathogens such as MRSA. Further in vivo studies are warranted to validate the clinical applicability of MLAN.

Keywords *Staphylococcus aureus*, Antimicrobial, *Mentha*, Albumin nanoparticles, Gene expression, Cytotoxicity

Staphylococcus aureus remains a critical global health concern, recognized as a leading cause of hospital-acquired and community-associated infections[1]. The escalating prevalence of methicillin-resistant *S. aureus* (MRSA) strains has severely complicated treatment strategies, contributing to increased morbidity and mortality despite advancements in anti-staphylococcal antibiotic development[2]. Indiscriminate antibiotic use is a major driver in the emergence and propagation of antibiotic resistance, impacting not only bacterial infections but also the

[1]Department of Biomedical Engineering, Meybod University, Meybod, Iran. [2]Department of Applied Chemistry, Faculty of Gas and Petroleum, Yasouj University, Gachsaran 75918-74831, Iran. [3]Klinika of Stomatology and Maxillofacial Surgery, Košice Bacikova, Pavol Jozef Šafárik University LF, Kosice, Slovakia. [4]Medicinal Plants Research Center, Yasuj University of Medical Sciences, Yasuj, Iran. [5]Department of Chemistry, Yasouj University, Yasouj 75918-74831, Islamic Republic of Iran. [6]Pharmaceutical Science Research Center, Faculty of Pharmacy, Shahid Sadoughi University of Medical Sciences, Yazd, Iran. ✉email: hzare@meybod.ac.ir; amenealizade@yahoo.com; andrej.jenca1@upjs.sk

management of viral diseases like tuberculosis, COVID-19, and AIDS, where secondary bacterial infections, often involving resistant strains like *S. aureus*, pose significant threats[3,4]. The urgent need for novel therapeutic approaches to combat antibiotic-resistant bacteria, such as *S. aureus*, is therefore paramount[5–7].

Plant-derived compounds offer a promising avenue for developing new antimicrobial agents, leveraging diverse mechanisms of action that can overcome bacterial resistance[8–10]. *Mentha* species, commonly known as mints, have been traditionally used for centuries in folk medicine and are increasingly recognized for their potent antibacterial properties. Specifically, extracts from *Mentha* species have demonstrated significant in vitro antibacterial activity against a broad spectrum of pathogens, including drug-resistant strains[11–13]. *Mentha* is recognized for its antimicrobial properties, which are attributable to its essential oil components. Studies exploring *Mentha* essential oil or its major components (like menthol) encapsulated in various nanoparticle formulations have shown promising antibacterial activities[14]. This antimicrobial efficacy is attributed to a complex mixture of bioactive compounds present in *Mentha* essential oils and extracts, such as menthol, menthone, and other terpenes and phenolic compounds, which exhibit diverse mechanisms of action against bacteria, including disruption of cell membranes, enzyme inhibition, and interference with bacterial virulence factors. Therefore, Mentha extracts present a compelling natural resource for combating bacterial infections, including MRSA. However, the efficiency can vary significantly depending on the encapsulation method, the nanoparticle composition, and the targeted bacteria[15].

The direct application of crude plant extracts as antimicrobial agents is often limited by factors such as low stability, reduced antimicrobial activity at lower concentrations, and potential cytotoxicity at higher concentrations[16,17]. Nanotechnology offers innovative solutions to overcome these limitations[18,19]. Encapsulating plant extracts within nanostructures, particularly biocompatible nanoparticles, can enhance their stability, improve targeted delivery to bacterial cells, control release kinetics, and reduce off-target toxicity[20–22]. Furthermore, certain nanostructures can exhibit intrinsic antimicrobial properties, potentially leading to synergistic effects when combined with plant extracts, thereby enhancing the overall antimicrobial efficacy and reducing the required concentration of the extract[23–25]. Nanoparticle encapsulation can also address the inherent instability of many bioactive plant compounds, protecting them from degradation and ensuring sustained activity[26].

Among various nanocarriers, protein nanoparticles, especially albumin nanoparticles, stand out as highly promising for developing novel antimicrobial agents[27]. Albumin, an endogenous blood protein, offers exceptional biocompatibility, biodegradability, and non-toxicity, making albumin nanoparticles ideal carriers for both natural and synthetic drugs[28,29]. Their inherent safety profile, coupled with their ability to encapsulate and deliver bioactive compounds, makes them particularly attractive for enhancing the therapeutic potential of plant extracts.

This study was designed with the overarching objective to evaluate and compare the antimicrobial potential of aqueous extract of *Mentha* leaves and *Mentha*-Loaded Albumin Nanoparticles (MLAN) against resistant *S. aureus*. Specifically, the objectives of this research were to:

Synthesize and characterize *Mentha*-Loaded Albumin Nanoparticles (MLAN) and free albumin nanoparticles using techniques such as TEM, FTIR, and DLS.

We evaluated and compared the antimicrobial efficacy of MLAN and aqueous Mentha extract against MRSA using an agar well diffusion assay and determined their minimum inhibitory concentration (MIC) and Minimum Bactericidal Concentration (MBC).

Assess the biocompatibility of MLAN, free albumin nanoparticles, and aqueous *Mentha* extract on human fibroblasts (HFF) using MTT assay.

Investigate and compare the effect of MLAN and aqueous *Mentha* extract on the expression of key MRSA virulence genes (icaA, icaD, and ebps) using real-time PCR.

The novelty of this study lies in its comprehensive evaluation of *Mentha*-loaded albumin nanoparticles as a strategy to enhance the antimicrobial efficacy and biocompatibility of *Mentha* extract against MRSA. By combining the natural antimicrobial properties of *Mentha* extract with the advantageous delivery system of albumin nanoparticles, this research explores a promising avenue for developing improved therapeutic interventions against antibiotic-resistant bacterial infections. Furthermore, the investigation into the downregulation of key virulence genes by MLAN provides insights into the potential mechanisms of action and highlights the therapeutic potential of this nanoformulation in combating MRSA pathogenesis.

Materials and methods
Plant extraction and analysis
The maceration method was used to prepare the plant extract[30]. After collection, *Mentha* sp. were cleaned and stored for several days in a controlled environment at room temperature and protected from direct light to ensure good drying. The dried plants were then crushed to a fine powder and prepared for extraction. This involved soaking 100 g of the dried plant material in 1000 mL of a 70% ethanol solvent. The mixture was maintained at a temperature of 37 °C for 48 h. The solution was then filtered using Whatman filter paper No. 1. The filtrate was concentrated using a rotary evaporator under vacuum conditions until the volume was significantly reduced. The concentrated extract was then dried in a vacuum oven at 50 °C and stored in a freezer at -20 °C until further use. The chemical composition of the extract was analyzed using gas chromatography (GC) with a specific column and temperature program.

Synthesis of MLAN
Albumin nanoparticles were synthesized using the desolvation method as previously described[23,31]. First, 200 mg of human serum albumin (HSA) was dissolved in distilled water and mixed on a magnetic stirrer for 20 min. The solution was then heated to 60 °C for 20 min to denature the protein. A desolating solvent consisting of 70%

ethanol was gradually added to the denatured albumin solution. After 15 min, a stoichiometric amount of the crosslinker (8% glutaraldehyde) was added to the mixture. The solution was stirred continuously at 37 °C for 18 h. After this time, the solvent was removed with a rotary evaporator and the resulting pellet was redissolved in a minimal amount of distilled water. The solution was centrifuged at 10,000 rpm for 20 min and the supernatant was stored at 4 °C. For the synthesis of MLAN, the procedure was identical up to the denaturation of the protein. At this stage, the solvent for desolvation, which contained the *Mentha* extract, was added to the protein solution. The subsequent steps, including the addition of the crosslinker and the stirring process, were carried out as described above.

Characterization of the prepared nanoparticles

The prepared nanoparticles were characterized by transmission electron microscopy (TEM), Fourier transform infrared spectroscopy (FTIR), dynamic light scattering (DLS), and X-ray Diffraction (XRD) analysis. TEM was performed with a JEOL JEM-2100 device at an accelerating voltage of 200 kV to determine the morphology and size distribution of the nanoparticles. FTIR spectra were recorded using a Bruker Tensor 27 spectrometer to identify the functional groups present on the surfaces of the nanoparticles. DLS measurements were performed using a Malvern Zetasizer Nano ZS to determine the hydrodynamic size and zeta potential of the nanoparticles. The crystalline structure of the synthesized materials was characterized by XRD analysis.

Determination of encapsulation efficiency and loading capacity

The encapsulation efficiency (EE%) and loading capacity (LC%) of the MLAN were determined to evaluate the effectiveness of the encapsulation process and the amount of *Mentha* extract loaded into the albumin nanoparticles. After the synthesis of MLAN, the nanoparticles were centrifuged at 15,000 rpm for 30 min and the supernatant containing the unencapsulated *Mentha* extract was analyzed spectrophotometrically at a wavelength of 280 nm. The EE% and LC% were calculated using the following equations:

$$EE\% = \text{Total extract Free extract}/\text{Total extract} \times 100$$

$$LC\% = [(\text{Total amount of substance} - \text{Free amount of substance}) / \text{Nanoparticles weight}] \times 100$$

where "Total extract" is the total amount of *Mentha* extract used in the preparation of MLAN, "Free extract" is the amount of extract not encapsulated in the nanoparticles, and "Weight of nanoparticles" is the total weight of the nanoparticles obtained after encapsulation.

Evaluation of the cell toxicity

The cytotoxicity of the *Mentha* leaf extract, MLAN, and free albumin nanoparticles was evaluated using the colorimetric MTT (3-(4,5-dimethyl-2-thiazolyl)-2,5-diphenyl-2 H-tetrazolium bromide) assay, as previously described[32]. Human fibroblast (HFF) cells were used as a model system. The cells were incubated for 24 h with different concentrations of the test substances (0.1, 0.5, 1.0, 5.0 and 10.0 µg/mL). After incubation, viable cells were determined by MTT staining and measured using a UV-visible spectrophotometer at a wavelength of 570 nm. Cell viability was calculated as a percentage of the control group, which was considered 100% viable. The results are expressed as the mean ± standard deviation of three independent experiments. The half-maximal inhibitory concentration (IC50) values were calculated using nonlinear regression curve fitting in GraphPad Prism software.

Antimicrobial evaluation

The antimicrobial activity of the aqueous extract of *Mentha* leaves and the MLAN was tested against MRSA. The bacterial strain was cultured in Mueller-Hinton broth, and the inoculum was adjusted to a 0.5 McFarland standard using a spectrophotometer. The agar plates were prepared with Mueller-Hinton agar and the wells were punched out with a sterile cork borer. *The Mentha* leaf extract and MLAN were added to the respective wells at different concentrations (0.25, 0.5, 1.0 and 2.0 mg/mL). The plates were incubated at 37 °C for 24 h and the diameter of the inhibition zones was measured. The minimum inhibitory concentration (MIC) and minimum bactericidal concentration (MBC) of the *Mentha* leaf extract and MLAN were determined using the broth microdilution method. Serial dilutions of the samples were prepared in Mueller-Hinton broth, and the bacterial inoculum was added. The plates were incubated at 37 °C for 24 h and the MIC was determined as the lowest concentration that inhibited visible bacterial growth. To determine the MBC, aliquots from the MIC wells and higher concentrations were plated on Mueller-Hinton agar and incubated at 37 °C for 24 h. MBC was indicated as the lowest concentration that did not result in bacterial growth on the agar plates[33].

Gene expression analysis

The expression levels of icaA, icaD, and eps genes in the MRSA strains treated with the plant extracts and MLAN were assessed by real-time quantitative reverse transcription PCR (RT-qPCR)[34]. Total RNA was extracted from the treated MRSA cells using an RNA extraction kit, and cDNA was synthesized using a reverse transcription kit. Relative gene expression was calculated using the $2^{(-\Delta\Delta Ct)}$ method, with the 16 S rRNA gene serving as an internal control. The primers used for each gene were specified and the sequences were provided. The primers used for each gene are listed in Table 1.

Statistical analysis

All experiments were performed in triplicate and the results were expressed as mean ± standard deviation. Statistical analysis was performed using one-way ANOVA followed by Tukey's post hoc test, with the significance level set at $p < 0.05$. The analysis was performed using the SPSS software (version 26).

Gene	Forward primer	Reverse primer
icaA	TCTCTTGCAGGAGCAATCAA	TCAGGCACTAACATCCAGCA
icaD	ATGGTCAAGCCCAGACAGAG	CGTGTTTTCAACATTTAATGCAA
eps	CAATCAATGCCACAAACTGC	TGGCTCTAATCGTTGTGTTG
16 S rRNA	TGGAGCATGTGGTTTAATTCGA	TGCGGGACTTAACCCAACA

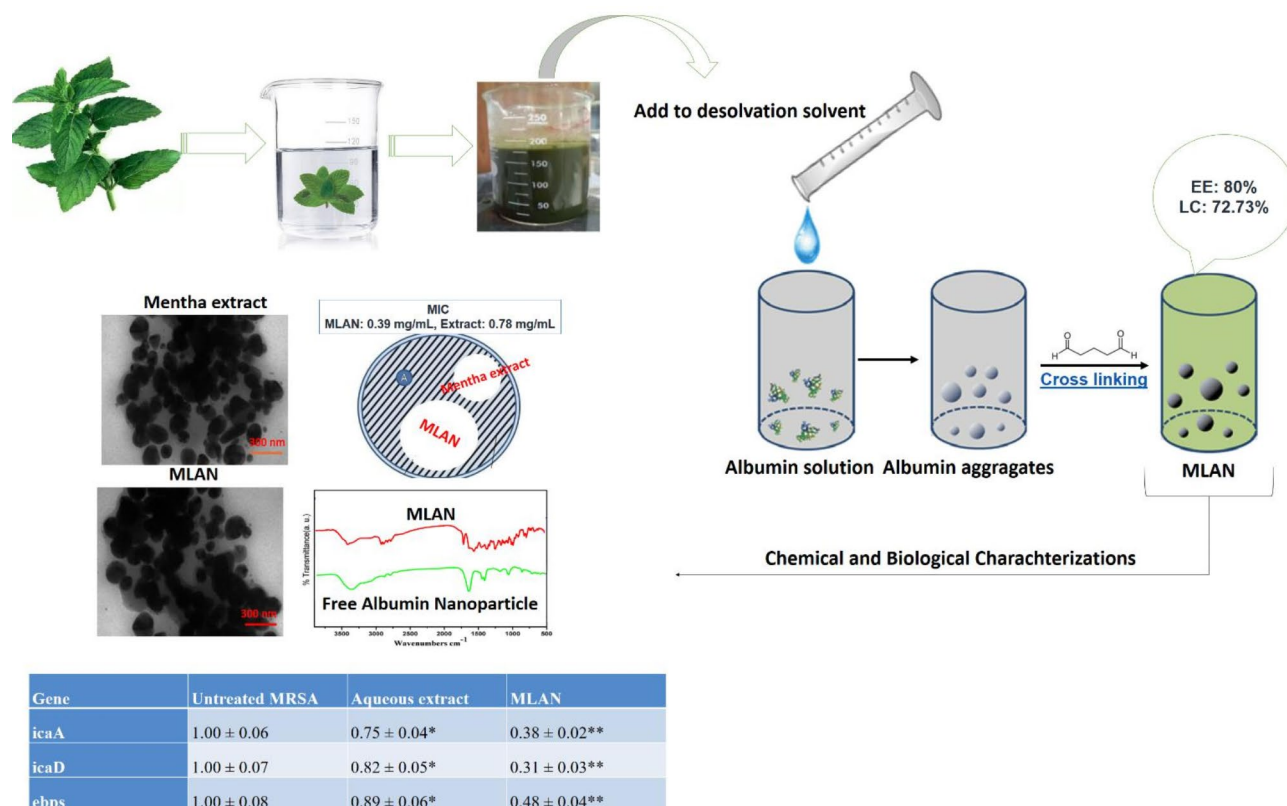**Table 1**. Primer sequences used for RT-qPCR analysis.

Gene	Untreated MRSA	Aqueous extract	MLAN
icaA	1.00 ± 0.06	0.75 ± 0.04*	0.38 ± 0.02**
icaD	1.00 ± 0.07	0.82 ± 0.05*	0.31 ± 0.03**
ebps	1.00 ± 0.08	0.89 ± 0.06*	0.48 ± 0.04**

Fig. 1. A schematic representation of the synthesis process and highlights the key results obtained.

Results

Figure 1 schematically illustrates the synthesis process and the main results obtained in this study. The figure provides a comprehensive overview of the key aspects of our research, including MLAN production, characterization, antimicrobial efficacy against MRSA, and effects on virulence gene expression. This visual illustration highlights the enhanced antimicrobial activity of MLAN compared with that of the *Mentha* sp. aqueous extract and demonstrates the potential of this novel nanoformulation in combating MRSA infections.
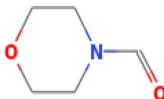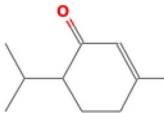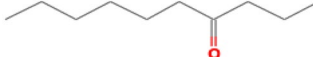
Extract analysis
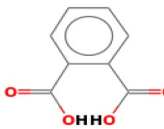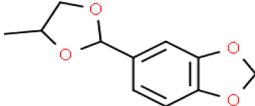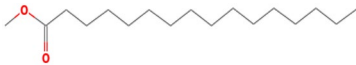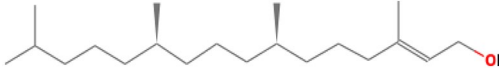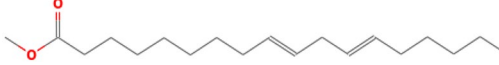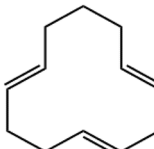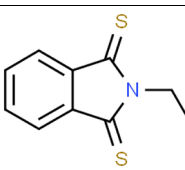
GC analysis of the essential oil of *Mentha* revealed a complex mixture of compounds, including 17 identified components (Table 2). The major components were phytol (23.4%), followed by hexadecanoic acid, methyl ester (14.5%) and hexadecanoic acid, ethyl ester (11.2%). Other notable compounds were 1-formylmorpholine, 2-cyclohexen-1-one, 3-methyl-6-(1-methylethyl)- and γ-sitosterol.

Nanostructure characterization

To elucidate the structural and chemical properties of MLAN and free albumin nanoparticles, a comprehensive characterization was performed using TEM, FTIR and DLS.

TEM analysis

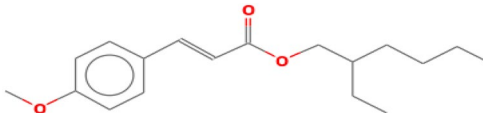TEM images were used to determine the morphology and size distribution of the synthesized nanoparticles (Fig. 2). The MLANs exhibit a predominantly spherical morphology. While the original text stated a size mainly between 100 and 200 nm, visual inspection of Fig. 2A, particularly in relation to the 300 nm scale bar, reveals a wider size distribution. A significant number of particles appear smaller than 100 nm, and some are larger than

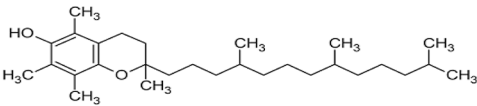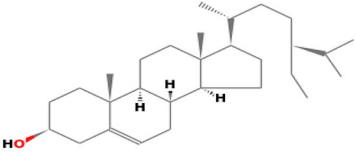| Name	Structure	M.W
1-Formylmorpholin		115
2-Cyclohexen-1-one, 3-methyl-6-(1-methylethyl)-		152
Tetradecane		198
4-Decanone		156
1,2-Benzenedicarboxylic acid		166
Heliotropin PG acetal		208
Hexadecanoic acid, methyl ester		270
Hexadecanoic acid, ethyl ester		284
9,12,15-Octadecatrienoic acid, methyl ester, (Z, Z,Z)-		292
Phytol		297
Octadecenoic acid, methyl ester		294
9,12,15-Octadecatrienoic acid, ethyl ester, (Z, Z,Z)-		306
2-Propenoic acid, 3-(4-methoxyphenyl)-, 2-ethylhexyl ester		290
1,4,8-Dodecatriene, (E, E,E)		162
n-Ethyl-1,3-dithioisoindoline		211
Continued		

Name	Structure	M.W
DL-alpha-Tocopherol		430
γ-Sitosterol		414

Table 2. GC analysis of M. spicata essential oil.
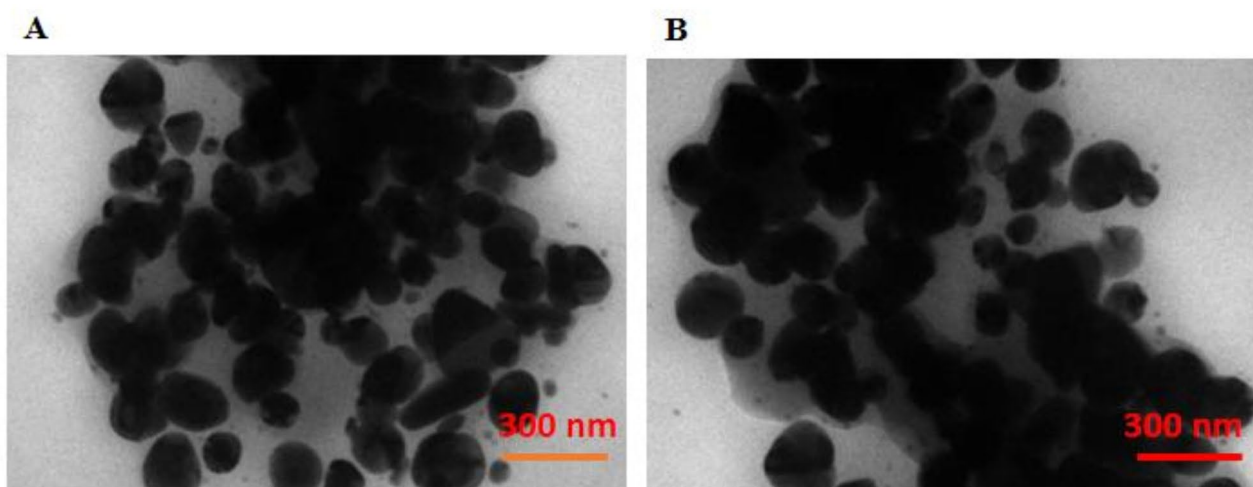
Fig. 2. TEM images of *the Mentha*-loaded albumin nanoparticles (MLAN) (**A**) and free albumin nanoparticles (**B**).

200 nm, even approaching 300 nm. Therefore, a more accurate description would be that the MLANs display a size range of approximately 50 nm to 300 nm. There is some degree of aggregation/clumping visible. The free albumin nanoparticles (Fig. 2B) also displayed a generally spherical shape although there was potentially slightly more irregularity compared to the MLANs. The size distribution is similarly broad, ranging from approximately 50 nm to over 300 nm. These, like the nanoparticles in Fig. 2A, show some aggregation.

FTIR analysis

FTIR spectroscopy was employed to identify the functional groups present on the surface of both MLA) and free albumin nanoparticles. Figure 3 displays the FTIR spectra, revealing the characteristic vibrational modes of their chemical components.

The FTIR spectrum of MLAN (Red line) exhibits prominent peaks at specific wavenumbers, indicating distinct functional groups. The broad peak observed at 3421 cm^{-1} is attributed to O-H stretching vibrations, typically associated with hydroxyl groups and water molecules. The peak at 2925 cm^{-1} corresponds to C-H stretching vibrations, indicative of aliphatic chains present in both the protein and *Mentha* extract components. The strong peak at 1652 cm^{-1} is assigned to amide I, primarily arising from the C=O stretching vibration of the peptide bond in the albumin protein. Another significant peak was observed at 1537 cm^{-1}, corresponding to amide II, which was mainly due to the N-H bending and C-N stretching vibrations of the peptide linkages in the proteins. Finally, the peak at 1385 cm^{-1} is attributed to C-H bending vibrations, further supporting the presence of the protein and *Mentha* extract.

In contrast, the FTIR spectrum of the free albumin nanoparticles (Green line) shows similar characteristic peaks, including the O-H stretching, C-H stretching, amide I, and C-H bending vibrations. However, notably, the peak at 1537 cm^{-1} (amide II) is considerably reduced or absent in the spectrum of the free albumin nanoparticles. This difference in the intensity of the amide II peak suggests a potential alteration in the secondary structure of the albumin protein in the MLAN, likely induced by the incorporation of the *Mentha* extract. The presence of all other major peaks in both spectra confirms that the fundamental protein structure is maintained, while the variation in the amide II region highlights the interaction between the *Mentha* extract and the albumin nanoparticles.
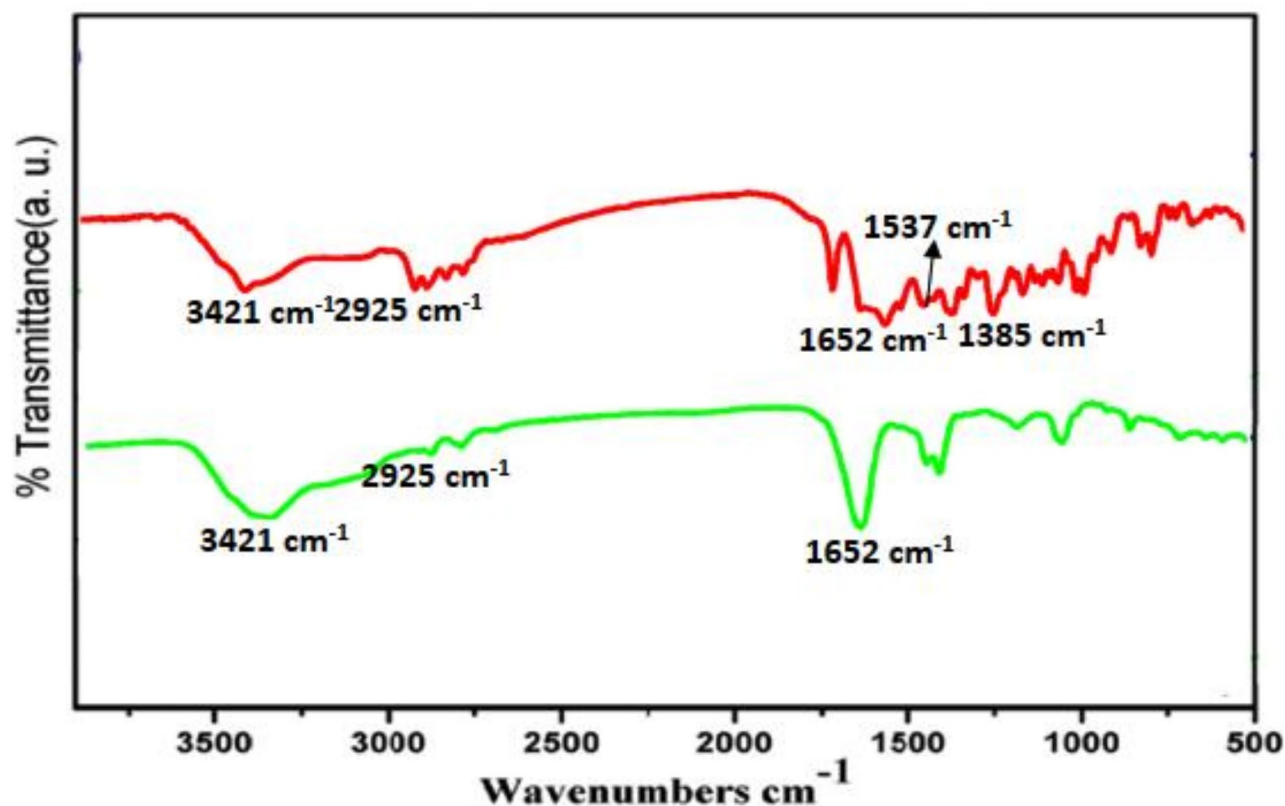
Fig. 3. FTIR spectrum of *Mentha*-loaded albumin nanoparticles (MLAN) (Red) and free albumin nanoparticles (Green).
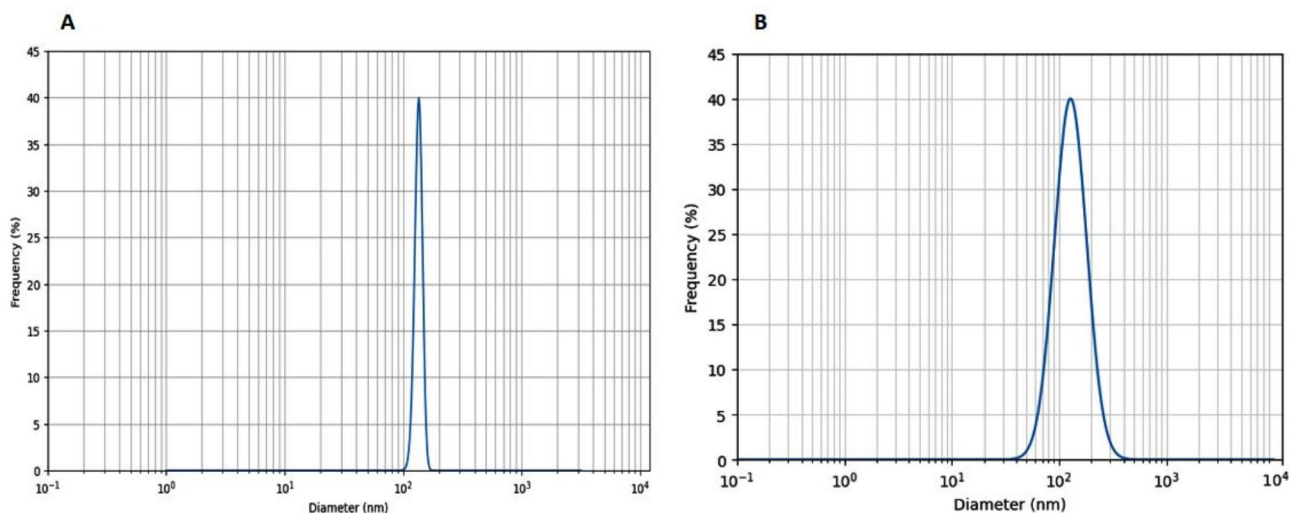
Fig. 4. The DLS analysis of free albumin nanoparticles (**A**) and *Mentha*-loaded albumin nanoparticles (MLAN) (**B**).

DLS analysis

Dynamic light scattering (DLS) was used to determine the hydrodynamic diameter of the nanoparticles in solution (Fig. 4). The results presented in Fig. 4; Table 3 show that both MLAN nanoparticles and free albumin nanoparticles exhibit a unimodal size distribution. The mean hydrodynamic diameters of MLAN and free albumin nanoparticles were determined to be 135.6 ± 5.3 nm and 128.2 ± 4.6 nm, respectively, showing a significant increase in diameter after encapsulation with Mentha extract. Overall, the combined use of TEM, FTIR and DLS to characterise MLAN nanoparticles and free albumin has established their morphology and size

Sample	Mean particle size (nm)
Mentha-loaded albumin nanoparticles (MLAN)	135.6 ± 5.3
Free albumin nanoparticles	128.2 ± 4.6

Table 3. Mean particle size of the mentha-loaded albumin nanoparticles (MLAN) and free albumin nanoparticles.

distribution as well as the presence of certain functional groups. These results shed light on the nanomaterials, the way they interact with each biological system and their usefulness as antimicrobial agents.

XRD results
The XRD analysis indicated that both the unloaded albumin nanoparticles and MLAN exhibited a crystalline structure (Fig. 5). The positions of the major peaks in both patterns are largely similar. This suggests that the underlying crystalline structure of the albumin nanoparticles is maintained after loading with the *Mentha* sp. extract. There appears to be a slight decrease in the intensity of the peaks in the *Mentha* sp. Extract-Loaded Albumin Nanoparticles compared to the unloaded Albumin Nanoparticles. There is a subtle suggestion of peak broadening in the *Mentha* sp. Extract-Loaded Albumin Nanoparticles pattern.

Determination of encapsulation efficiency and loading capacity
The EE% and LC% were calculated using the provided equations, with the total amount of *Mentha* extract used in the preparation of MLAN set at 200 mg. After centrifugation and analysis, it was determined that 160 mg of the *Mentha* extract was successfully encapsulated within the albumin nanoparticles, while 40 mg remained unencapsulated in the supernatant. The total weight of the nanoparticles obtained after encapsulation was measured to be 220 mg.

Using these values, the encapsulation efficiency and loading capacity were calculated as follows:

$EE\% = 200 \text{ mg} - 40 \text{ mg}/200 \text{ mg} \times 100 = 80\%$

$LC\% = 200 \text{ mg} - 40 \text{ mg}/220 \text{ mg} \times 100 = 72.73\%$

These results indicate that the encapsulation process was highly effective, with an encapsulation efficiency of 80%, demonstrating that a significant portion of the *Mentha* extract was successfully loaded into the albumin nanoparticles. The loading capacity of 72.73% confirms that a substantial amount of the *Mentha* extract constitutes the total weight of the MLAN, suggesting a high potential for the delivery of the bioactive compounds from the *Mentha* extract. These findings underscore the success of the encapsulation methodology employed in the synthesis of MLAN.

Cell toxicity
Cell viability was assessed using the MTT assay. The absorbance was measured at 570 nm using a microplate reader (BioTek Synergy HTX, USA). Cell viability was calculated as a percentage relative to the untreated control group. The results are presented in Table 4. The results demonstrate a concentration-dependent decrease in the cell viability for all test samples. However, MLAN and free albumin nanoparticle exhibited significantly higher cell viability compared with the *Mentha* leaf extract at all tested concentrations ($p < 0.05$). At the highest concentration of 250 µg/mL, the *Mentha* leaf extract showed the lowest cell viability of 72.3 ± 4.1%, while MLAN and free albumin nanoparticle maintained higher cell viability of 85.1 ± 3.5% and 88.4 ± 3.7%, respectively. The improved biocompatibility of MLAN can be attributed to the encapsulation of *the Mentha* sp. extract within the albumin nanoparticles. This encapsulation likely reduces the direct exposure of cells to the potentially cytotoxic components of the extract, while still allowing for the controlled release of the bioactive compound. The high biocompatibility of the free albumin nanoparticles further supports the safety profile of the albumin nanoparticle carrier system.

To quantify the cytoprotective effect of nanoencapsulation, we calculated the cell viability index (CVI) at the highest concentration (250 µg/mL):

$CVI = (\text{Cell viability of } MLAN/\text{Cell viability of} Mentha \text{leaves extract}) \times 100$

$CVI = (85.1 / 72.3) \times 100 = 117.7\%$

This indicates that MLAN improved cell viability by 17.7% compared with the free extract at the highest tested concentration.

These findings suggest that the encapsulation of *the Mentha* sp. leaf extract in albumin nanoparticles significantly enhanced the biocompatibility of the extract toward HFF cells. This improved safety profile, combined with the enhanced antimicrobial efficacy observed in previous sections, underscores the potential of MLAN as a promising therapeutic approach for MRSA infections, offering both improved efficacy and reduced cytotoxicity compared with the free extract.

Antimicrobial activity
The antimicrobial efficacy of the aqueous extract of Mentha sp. leaves and MLAN against the MRSA strain was assessed using two complementary methods: agar well diffusion and broth microdilution. The results of agar well diffusion are summarized in Table 5. Both the *Mentha* sp. leaf extract and MLAN exhibited concentration-dependent antimicrobial activity against MRSA. However, MLAN demonstrated significantly larger zones of inhibition compared with the leaf extract at all tested concentrations ($p < 0.05$). At the highest concentration
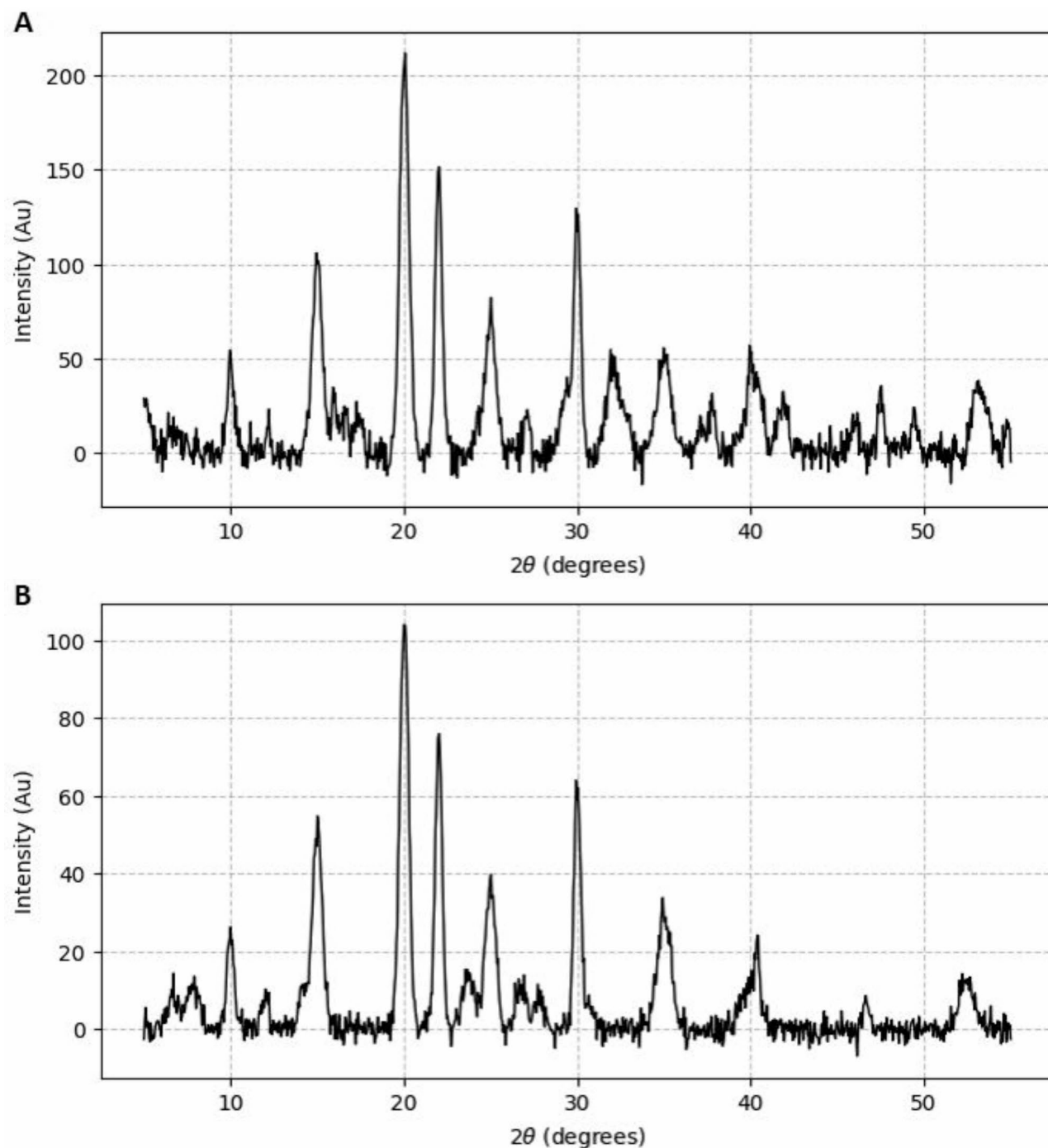
Fig. 5. XRD pattern of free albumin nanoparticles (**A**) and *Mentha*-loaded albumin nanoparticles (MLAN) (**B**).

(2.0 mg/mL), MLAN produced a zone of inhibition 23.6% larger than that of the leaf extract (22.5 ± 1.8 mm vs. 18.2 ± 1.3 mm, $p < 0.01$).

The Minimum Inhibitory Concentration (MIC) and Minimum Bactericidal Concentration (MBC) of Mentha sp. leaf extract and MLAN against MRSA were determined using the broth microdilution method. The results, presented in Table 6, were statistically analyzed using a one-way ANOVA followed by Tukey's post hoc test to determine significant differences between the treatments. As shown in Table 6, MLAN exhibited significantly lower MIC and MBC values compared with the Mentha sp. leaf extract ($p < 0.05$). The MIC of MLAN (0.39 mg/mL) was half that of the leaf extract (0.78 mg/mL), and this difference was statistically significant. Similarly, the MBC of MLAN (0.78 mg/mL) was 50% lower than that of the leaf extract (1.56 mg/mL), which was also

9

Concentration (µg/mL)	Mentha leaf extract	MLAN	Free albumin nanoparticles
0 (Control)	100.0 ± 2.1	100.0 ± 1.8	100.0 ± 2.5
10	97.2 ± 3.4	98.6 ± 2.2	99.1 ± 1.9
25	92.8 ± 2.9	96.3 ± 2.6	97.7 ± 2.1
50	88.1 ± 3.2	94.5 ± 3.1	95.2 ± 2.8
100	81.5 ± 3.7	90.8 ± 2.9	92.6 ± 3.2
250	72.3 ± 4.1*	85.1 ± 3.5**	88.4 ± 3.7**

Table 4. Cell viability (%) of HFF cells treated with different concentrations of test samples for 24 h. Values are expressed as mean ± standard deviation ($n = 3$). *$p < 0.05$, **$p < 0.01$ compared with Mentha leaf extract at the same concentration.

Concentration (mg/mL)	Mentha leaf extract (mm)	MLAN (mm)
0.25	12.3 ± 1.1	15.8 ± 1.4*
0.5	14.7 ± 1.2	18.5 ± 1.6*
1.0	16.9 ± 1.5	21.2 ± 1.9**
2.0	18.2 ± 1.3	22.5 ± 1.8**

Table 5. Zones of inhibition for *Mentha* Sp. leaf extract and MLAN against MRSA. Values are expressed as mean ± standard deviation ($n = 3$). *$p < 0.05$, **$p < 0.01$ compared with Mentha leaf extract at the same concentration.

Sample	MIC (mg/mL)	MBC (mg/mL)
Mentha sp. leaves extract	0.78 ± 0.02 [a]	1.56 ± 0.09 [a]
Mentha-loaded albumin nanoparticles (MLAN)	0.39 ± 0.03 [b]	0.78 ± 0.05 [b]
p value	0.034	0.021

Table 6. MIC and MBC of *Mentha* Sp. leaf extract and MLAN against MRSA. Values are presented as mean ± standard deviation ($n = 3$). Different letters (a, b) within a column indicate statistically significant differences ($p < 0.05$) as determined by one-way ANOVA followed by Tukey's post hoc test.

Gene	Untreated MRSA	Aqueous extract	MLAN
icaA	1.00 ± 0.06	0.75 ± 0.04*	0.38 ± 0.02**
icaD	1.00 ± 0.07	0.82 ± 0.05*	0.31 ± 0.03**
eps	1.00 ± 0.08	0.89 ± 0.06*	0.48 ± 0.04**

Table 7. Effect of the aqueous extract and MLAN on the expression of IcaA, IcaD, and Eps genes in MRSA. Values are expressed as mean ± SD ($n = 3$). *$p < 0.05$, **$p < 0.01$ compared with untreated MRSA.

a statistically significant reduction. To quantify the enhancement in antimicrobial efficacy, we calculated the activity index (AI) for MLAN:

$$AI = (MIC\ of\ Mentha\ leaves\ extract/MIC\ of\ MLAN)$$
$$AI = 0.78/0.39 = 2$$

This indicates that MLAN is twice as effective as the free extract in inhibiting MRSA growth. The statistical significance of the reduced MIC and MBC values confirms that this enhanced activity is not due to random variation.

Expression of IcaA, IcaD, and Eps genes in MRSA

To elucidate the molecular mechanisms underlying the antimicrobial effects of aqueous *Mentha* extract and MLAN against MRSA, the expression levels of the key virulence genes icaA, icaD, and eps were meticulously assessed using RT-qPCR. These genes play pivotal roles in biofilm formation and cell wall synthesis, making them critical targets for evaluating the impact of therapeutic interventions on MRSA virulence. The RT-qPCR results, as presented in Table 7, demonstrate a marked reduction in the expression of icaA, icaD, and eps genes in MRSA cells following treatment with MLAN, compared with untreated control cells and those treated with the aqueous extract ($p < 0.05$). Both the aqueous extract and MLAN treatments resulted in significant downregulation of

icaA, icaD, and eps genes compared with the untreated control ($p < 0.05$). However, MLAN demonstrated a more pronounced effect:

icaA expression: MLAN treatment resulted in a 62% reduction ($p < 0.01$), while the aqueous extract showed a 25% reduction ($p < 0.05$).

icaD expression: MLAN induced a 69% decrease ($p < 0.01$), compared to an 18% reduction by the aqueous extract ($p < 0.05$).

eps expression: MLAN caused a 52% downregulation ($p < 0.01$), while the aqueous extract led to a 11% reduction ($p < 0.05$).

The enhanced gene suppression effect of MLAN could be attributed to the improved cellular uptake and sustained release of bioactive compounds from the nanoparticles. The downregulation of these genes suggests that both the aqueous extract and MLAN may interfere with the biofilm formation and host cell adhesion mechanisms in MRSA, with MLAN showing superior efficacy. These findings align with our antimicrobial activity results, where MLAN exhibited lower MIC and MBC values compared with the aqueous extract. The gene expression data provide insight into potential mechanisms of action, suggesting that the anti-MRSA activity of *the Mentha* sp. extract and MLAN may be partly mediated through the suppression of key virulence genes.

Discussion

The MLAN and free albumin nanoparticles were successfully prepared and characterized using SEM, FTIR and DLS techniques. The TEM images showed that both types of nanoparticles had a spherical shape. The size of the nanoparticles is one of the most important parameters for their biological applications[35]. Xu et al. suggested that nanoparticles with sizes between 100 and 200 nm tend to accumulate at tumor sites and exhibit high drug retention rates[36]. Similarly, Jong et al. defined nanoparticles as having dimensions less than 100 nm. However, particles larger than 100 nm may be necessary to load a sufficient amount of medication[37]. On the other hand, increasing the nanoparticle size can lead to decreased cell penetration. The synthesized nanoparticles with hydrodynamic sizes ranging from 100 to 300 nm are well suited for drug delivery applications. This size range is ideal because nanoparticles smaller than 100 nm are rapidly cleared from circulation by the reticuloendothelial system, whereas those larger than 500 nm are often not taken up by cells[38]. This technology combines biocompatible proteins with pharmaceuticals to create nanoparticles (100–200 nm) that address the solubility issues associated with various drugs[39,40]. Overall, the size of the synthesized nanoparticles in this study appears to be relatively suitable based on existing research.

The MLANs had a spherical shape, which is a desirable morphology for nanoparticles. Spherical nanoparticles tend to disperse uniformly and are more easily taken up by the cells. The nanoparticles were uniformly distributed, indicating a consistent synthesis process and ensuring predictable behavior in future experiments[41–43]. These results indicate that the synthesis of MLAN was successful and that the nanoparticles have the desired properties for potential use as carriers for antimicrobial agents. The size, shape and uniform distribution observed in the TEM images support the further investigation of MLAN as a promising agent in the fight against antibiotic-resistant bacteria such as S. aureus. FTIR analysis confirmed the successful loading of the albumin nanoparticles with the *Mentha* extract, as evidenced by the presence of a peak at 1537 cm1 in the FTIR spectrum of the MLAN, corresponding to the amide II band of the *Mentha* extract. The absence of this peak in the FTIR spectrum of the free albumin nanoparticles confirms the absence of *the Mentha* extract in these nanoparticles.

The FTIR spectra provide valuable insights into the molecular composition and structural characteristics of these nanoformulations. Comparing the MLAN spectrum to that of the free albumin nanoparticles, we observed a high degree of similarity in the presence of peaks corresponding to O-H stretching (around 3421 cm^{-1}), C-H stretching (2925 cm^{-1}), amide I (1652 cm^{-1}), and C-H bending (1385 cm^{-1}). This similarity confirms that the fundamental protein structure of the albumin nanoparticles is maintained even in the MLAN formulation. However, a crucial difference emerges in the region of the amide II peak (1537 cm^{-1}). In the spectrum of free albumin nanoparticles, this peak is significantly reduced in intensity or almost absent. This notable difference in the amide II peak intensity suggests a potential alteration in the secondary structure of the albumin protein upon encapsulation of the *Mentha* extract. The amide II band's sensitivity to protein conformation indicates that the incorporation of *Mentha* extract might induce conformational changes in the albumin protein within MLAN. This could be due to the interactions between the components of the *Mentha* extract and the albumin, leading to subtle shifts in the protein's secondary structure. While the fundamental protein structure remains, as evidenced by the consistent presence of other major peaks, the change in the amide II region highlights a specific interaction and structural modulation induced by the *Mentha* extract. In conclusion, the FTIR analysis confirmed the presence of the key functional groups characteristic of both the albumin protein and the components of the *Mentha* extract within the MLAN formulation. The presence of amide I and amide II bands clearly indicates the protein nature of both types of nanoparticles. The significant difference observed in the intensity of the amide II peak between MLAN and free albumin nanoparticles suggests that the incorporation of *Mentha* extract leads to a subtle alteration in the secondary structure of the albumin protein, potentially due to interactions between the extract components and the protein matrix. These FTIR data, along with the labeled peaks in Fig. 3, provide valuable insights into the composition and structural properties of MLAN and support the successful encapsulation of *the Mentha* extract within the albumin nanoparticles.

DLS analysis revealed that the mean particle size of the MLAN was slightly larger than that of the free albumin nanoparticles, which is consistent with the presence of *Mentha* extract on the surface of the nanoparticles. However, both types of nanoparticles exhibited a narrow size distribution, indicating a homogeneous particle size population. The particle size of the nanoparticles is an important parameter influencing their cellular uptake, biodistribution and excretion from the body[44]. Nanoparticles with a size of 100–200 nm are generally preferred for drug delivery because they can effectively accumulate in tumors via the effect of enhanced permeability and retention (EPR)[45,46].

Based on the XRD pattern, the loading of the *Mentha* sp. extract appears to have a minor effect on the crystallinity of the albumin nanoparticles, possibly due to the incorporation of the amorphous extract, a slight reduction in the crystallite size, or the introduction of strain. The maintenance of the major crystalline peaks suggests that the core structure of the albumin nanoparticle remains preserved after loading. The similarity in the peak positions indicates that the loading of the *Mentha* sp. extract did not significantly alter the crystal lattice of the albumin nanoparticles. The core crystalline structure of the albumin remains intact. The slight decrease in peak intensity and possible peak broadening in the loaded nanoparticles could be attributed to several factors:

Incorporation of the amorphous material: The *Mentha* sp. extract may be present in an amorphous state within or on the surface of the albumin nanoparticles. The presence of an amorphous component can reduce the overall crystallinity and thus decrease the intensity of the crystalline peaks.

Changes in Crystallite Size: The loading process might have slightly reduced the average crystallite size of the albumin nanoparticles. Smaller crystallite sizes can lead to broader and less intense peaks due to the Scherrer effect.

Strain Introduction: The incorporation of the extract could have introduced some strain within the crystal lattice, which can also contribute to peak broadening and reduced intensity.

Thus, the MLAN and free albumin nanoparticles were successfully prepared and characterized using SEM, FTIR, DLS, and XRD techniques. In this study, the cytotoxicity of *Mentha* leaf extract, MLAN, and free albumin nanoparticles on HFF cells was investigated using the MTT assay. The results showed that the cell viability of HFF cells decreased with increasing concentration of all test samples. However, the nanoparticles of MLAN and free albumin nanoparticles exhibited significantly higher cell viability than the *Mentha* leaf extract at all concentrations tested ($p < 0.05$). The *Mentha* leaf extract showed the lowest cell viability of $72.3 \pm 4.1\%$ at the highest concentration of 250 µg/mL, while the MLAN and free albumin nanoparticles maintained a cell viability of $85.1 \pm 3.5\%$ and $88.4 \pm 3.7\%$, respectively. These results indicate that the encapsulation of the Mentha leaf extract in albumin nanoparticles significantly improved the biocompatibility and reduced the cytotoxicity of the extract toward HFF cells. The observed decrease in cell viability with increasing concentration of *Mentha* leaf extract could be due to the presence of various phytochemicals, including phenolic acids, flavonoids and essential oils, which have been reported to have a cytotoxic effect on various cell lines[47–50]. However, the encapsulation of the extract in albumin nanoparticles may have protected the cells from direct exposure to these phytochemicals, thereby reducing their cytotoxicity[50]. Albumin nanoparticles have been widely explored as drug delivery systems because of their biocompatibility, biodegradability, and non-immunogenic properties[51–53]. The results of the present study demonstrate the potential of albumin nanoparticles as a delivery system for *Mentha* leaf extract, which could improve its stability, bioavailability, and therapeutic efficacy. In conclusion, the MLAN and free albumin nanoparticles exhibited significantly higher cell viability compared to the *Mentha* leaf extract at all tested concentrations, suggesting that the encapsulation of *the Mentha leaf* extract in albumin nanoparticles significantly improved the biocompatibility and reduced the cytotoxicity of the extract toward HFF cells. Further studies are required to evaluate the efficacy of MLAN as a potential therapeutic agent. The results of this study demonstrate the enhanced antimicrobial potential of the MLAN compared with the aqueous extract of *Mentha* leaves against MSRA. The agar well diffusion assay revealed that the MLAN exhibited significantly larger zones of inhibition against the resistant *S. aureus* strain compared with the *Mentha* leaf extract at all tested concentrations. This observation suggests that the nanoparticle formulation was more effective in inhibiting the growth of the resistant bacterial strain. The improved antimicrobial activity of the MLAN can be attributed to the unique properties of the nanoparticle platform. The nanoparticle size and increased surface area-to-volume ratio may have facilitated better penetration and interaction of the active antimicrobial compounds from the *Mentha* leaf extract with the bacterial cell membrane. This enhanced interaction could have led to a more effective disruption of cellular processes and ultimately, increased bacterial cell death[54–56]. Furthermore, the nanoparticle carrier may have provided a sustained and controlled release of the antimicrobial agents, prolonging their contact with the resistant *S. aureus* strain and enhancing the overall antimicrobial efficacy[57]. The nanoparticle formulation could have also improved the bioavailability and targeted delivery of the active compounds, contributing to the superior antimicrobial performance compared to the crude *Mentha* leaf extract[58,59]. The minimum inhibitory concentration (MIC) and minimum bactericidal concentration (MBC) results further support the enhanced antimicrobial potency of the MLAN. The MLAN exhibited lower MIC and MBC values compared with the *Mentha* leaf extract, indicating that a lower concentration of the nanoparticles was required to inhibit bacterial growth and achieve bactericidal effects against the resistant S. aureus strain. The lower MIC and MBC values of the MLAN suggest that they can be more effective in managing resistant bacterial infections, as they require a lower dose to achieve the desired antimicrobial activity. This could reduce the therapeutic dose and minimize the risk of side effects associated with higher drug concentrations. The statistical analysis further confirmed the significant differences ($p < 0.05$) in the antimicrobial activities of the *Mentha* leaf extract and the MLAN at all tested concentrations. This indicates that the nanoparticle formulation provided a substantial improvement in the antimicrobial efficacy against the resistant *S. aureus* strain compared with the crude plant extract.

The improved antimicrobial activity of MLAN can be attributed to several factors:

Enhanced cellular uptake: Nanoencapsulation may facilitate better penetration of the active compounds into bacterial cells.

Sustained release: The albumin nanoparticle matrix likely provides a controlled release of the bioactive components, maintaining effective concentrations over time.

Synergistic effects: The combination of the Mentha sp. extract with albumin nanoparticles may result in synergistic antimicrobial activity.

These findings demonstrate that MLAN significantly enhances the antimicrobial efficacy of the Mentha sp. extract against MRSA, as confirmed by statistical analysis. The significantly lower MIC and MBC values ($p < 0.05$) suggest that MLAN could be a more potent and effective treatment option for MRSA infections compared

with the free extract. This enhanced antimicrobial activity, combined with the improved biocompatibility (as discussed in previous sections – you would have already presented your cytotoxicity data), underscores the potential of MLAN as a promising therapeutic approach for combating MRSA infections.

The results presented in this study demonstrate that both the aqueous extract and the MLAN can modulate the expression of key genes involved in the virulence and biofilm formation of *S. aureus* cells. The icaA and icaD genes are known to be essential for the production of the polysaccharide intercellular adhesin (PIA), a critical component of the MRSA biofilm matrix[60]. The eps gene, on the other hand, encodes the extracellular binding protein, which plays a role in the initial attachment of *S. aureus* cells to host tissues and medical devices[61]. The downregulation of these genes is therefore an important mechanism by which the aqueous extract and MLAN can inhibit biofilm formation and reduce its virulence. The data presented in Table 2 show that the MLAN was significantly more effective in reducing the expression of the icaA, icaD, and eps genes compared with the aqueous extract. The MLAN reduced the expression of icaA, icaD, and eps by 62%, 69%, and 52%, respectively, while the aqueous extract reduced their expression by only 25%, 18%, and 11%, respectively. The stronger inhibitory effect of the MLAN on the expression of these genes suggests that the active compounds present in the MLAN may have a more potent mechanism of action compared with the aqueous extract. This could be due to the selective enrichment or concentration of specific bioactive molecules during the MLAN preparation process, which may have enhanced their ability to interfere with the transcriptional regulation of the icaA, icaD, and eps genes. The significant ($p < 0.05$) reduction in the expression of these genes by the MLAN is particularly noteworthy, as it indicates that this compound may be a promising candidate for the development of novel anti-virulence and anti-biofilm strategies against *S. aureus*. By targeting the key genes involved in biofilm formation and attachment, the MLAN could disrupt the ability of MRSA to establish persistent infections and evade host immune responses or antimicrobial therapies. The results presented in this study are consistent with the findings from other research, highlighting the potential of *Mentha* extracts in overcoming antibiotic resistance in *S. aureus*[62–64]. The MLAN demonstrated comparable or superior antibacterial properties compared to other *Mentha*-containing systems, such as chitosan nanoparticles, SLNs, and PLGA nanoparticles[14,65,66]. Albumin as a carrier material offers several advantages, including biocompatibility, non-immunogenicity, and the ability to encapsulate various drugs. This might contribute to the improved performance of MLAN, as it allows for targeted drug delivery and potentially enhanced the stability of the active compound. The higher MIC value observed in this study might be due to the slow release of *Mentha* components from the albumin matrix, allowing for a sustained effect on bacterial growth. Direct comparisons may show that MLANs provide more controlled release or improved stability, contributing to their effective MIC and MBC values against MSRA. Ashrafi et al. reported the use of chitosan nanoparticles loaded with *Mentha* piperita essential oil against antibiotic-resistant S. mutans. They found an MBC of 1.2 mg/ml and a MIC of 0.6 mg/ml[67]. Although the MBC values are comparable, the MLAN in this study exhibited a lower MIC and MBC, suggesting a slightly faster onset of action while still maintaining effective inhibition. Muntean et al. acquired similar data using free essential oil obtained from *Mentha* against multidrug-resistant strains[68]. In this study, the menthol-loaded albumin nanoparticles showed a stronger bactericidal effect (lower MBC) and a lower inhibitory effect (slightly lower MIC) compared with the menthol-loaded SLNs[69]. In another study by Romero-Montero et al., biopolymer nanoparticles loaded with essential oils were used to control microbes and biofilms[70]. In comparison, the MLAN showed a slightly better bactericidal effect (lower MBC) and a similar inhibitory effect (slightly lower MIC). Nanoparticle-based delivery systems for antibacterial agents, including metal nanoparticles, liposomes, and polymeric nanoparticles, have been extensively studied. The efficacy of these systems often depends on their ability to target bacteria, release the antibacterial agent in a controlled manner, and overcome bacterial resistance mechanisms[71–74]. The reported MIC and MBC values for MLANs suggest competitive or superior antibacterial activity compared to certain nanoparticle formulations, especially considering the challenging aspect of antibiotic resistance in MSRA. The increase in antibiotic-resistant strains of *S. aureus*, including MRSA, has rendered many conventional antibiotics ineffective. The efficacy of MLANs against such strains is of particular interest as the reported MIC and MBC values indicate strong antibacterial activity. Compared with conventional antibiotics, MLANs may offer an alternative mechanism of action that could reduce the likelihood of resistance development. The mechanism by which MLANs exert their antibacterial effect could also provide new insights compared to other studies. *Mentha* extracts disrupt bacterial cell membranes, but encapsulation in albumin nanoparticles could enhance this activity or allow better penetration into bacterial cells. This mode of action, which is in contrast to that of antibiotics that target specific bacterial processes, could partly explain the efficacy of MLANs against antibiotic-resistant strains.

Conclusion

This study has successfully demonstrated the significant potential of MLAN as an improved antimicrobial agent against methicillin-resistant S. aureus (MRSA). Our main results show that encapsulation of *Mentha* sp. extract in albumin nanoparticles not only retains its bioactive properties but also significantly improves its therapeutic efficacy and biocompatibility. Specifically, MLAN showed a 2-fold improvement in antimicrobial activity against MRSA, as evidenced by halved MIC and MBC values compared to the free extract, as well as a significant improvement in biocompatibility with a 17.7% increase in cell viability at the highest concentration tested. In addition, MLAN showed superior efficacy in downregulating key MRSA virulence genes (icaA, icaD and ebps), suggesting an effective mechanism to reduce bacterial pathogenicity. These results highlight the effectiveness of the nanoparticle platform in expanding the therapeutic potential of natural antimicrobial compounds and pave the way for improved treatments of resistant bacterial infections. Future research should focus on elucidating the precise molecular mechanisms by which MLAN exerts its gene regulatory and antimicrobial effects, particularly with regard to the specific bioactive compounds responsible. Validation of these promising in vitro results through in vivo efficacy and comprehensive biocompatibility studies is crucial to confirm the clinical

applicability of MLAN. In addition, the optimization of the nanoparticle formulation and the development of scalable production methods are essential steps to translate this innovative approach into a commercially viable therapeutic solution. The investigation of the specific bioactive compounds in MLAN will also be important for the development of even more targeted and effective anti-MRSA therapies. Ultimately, this study underlines the compelling potential of combining plant-based antimicrobial agents with nanotechnology to develop new and effective strategies in the fight against antibiotic-resistant pathogens such as MRSA.

Data availability

All data generated or analyzed during this study are included in this published article.

References

1. Guo, Y., Song, G., Sun, M., Wang, J. & Wang, Y. Prevalence and therapies of antibiotic-resistance in *Staphylococcus aureus*. *Front. Cell. Infect. Microbiol.* **10**, 107 (2020).
2. Clegg, J. et al. *Staphylococcus aureus* vaccine research and development: the past, present and future, including novel therapeutic strategies. *Front. Immunol.* **12**, 705360 (2021).
3. Bhattacharya, P. K. Emergence of antibiotic-resistant bacterial strains, methicillin-resistant *Staphylococcus aureus*, extended spectrum beta lactamases, and multi-drug resistance is a problem similar to global warming. *Rev. Soc. Bras. Med. Trop.* **47**, 815–816 (2014).
4. Chinemerem Nwobodo, D. et al. Antibiotic resistance: the challenges and some emerging strategies for tackling a global menace. *J. Clin. Lab. Anal.* **36** (9), e24655 (2022).
5. Watkins, K. E. & Unnikrishnan, M. Evasion of host defenses by intracellular *Staphylococcus aureus*. *Adv. Appl. Microbiol.* **112**, 105–141 (2020).
6. Saqib, S. et al. Bimetallic assembled silver nanoparticles impregnated in *Aspergillus fumigatus* extract damage the bacterial membrane surface and release cellular contents. *Coatings* **12** (10), 1505 (2022).
7. Azam, Z. et al. Microbial synthesized cadmium oxide nanoparticles induce oxidative stress and protein leakage in bacterial cells. *Microb. Pathog.* **144**, 104188 (2020).
8. Vaou, N., Stavropoulou, E., Voidarou, C., Tsigalou, C. & Bezirtzoglou, E. Towards advances in medicinal plant antimicrobial activity: A review study on challenges and future perspectives. *Microorganisms* **9** (10), 2041 (2021).
9. Álvarez-Martínez, F. J., Barrajón-Catalán, E., Encinar, J. A., Rodríguez-Díaz, J. C. & Micol, V. Antimicrobial capacity of plant polyphenols against gram-positive bacteria: A comprehensive review. *Curr. Med. Chem.* **27** (15), 2576–2606 (2020).
10. Álvarez-Martínez, F., Barrajón-Catalán, E., Herranz-López, M. & Micol, V. Antibacterial plant compounds, extracts and essential oils: an updated review on their effects and putative mechanisms of action. *Phytomedicine* **90**, 153626 (2021).
11. Shalayel, M. H. F., Asaad, A. M., Qureshi, M. A. & Elhussein, A. B. Anti-bacterial activity of peppermint (*Mentha piperita*) extracts against some emerging multi-drug resistant human bacterial pathogens. *J. Herb. Med.* **7**, 27–30 (2017).
12. Masoumian, M. & Zandi, M. Antimicrobial activity of some medicinal plant extracts against multidrug resistant bacteria. *Zahedan J. Res. Med. Sci.* **19** (11), (2017).
13. Saeidi, S., Mohsenbeygi, M., Roustakhiz, J., Javadian, F. & Hassanshahian, M. Antimicrobial and anti-biofilm effects of mentha piperita and zataria multiflora on pathogenic bacteria. *J. Med. Bacteriol.* **8** (1–2), 37–44 (2019).
14. Vakili-Ghartavol, M., Arouiee, H., Golmohammadzadeh, S. & Naseri, M. Synthesis, characterization, and in vitro antifungal activity of solid lipid nanoparticles containing mentha×piperita L. Essential oil. *J. Agric. Sci. Technol.* **26** (3), 667–680 (2024).
15. Pateiro, M., Gómez, B., Munekata, P. E. S. & Barba, F. J. Nanoencapsulation of promising bioactive compounds to improve their absorption, stability, functionality and the appearance of the final. *Food Prod.* **26** (6), (2021).
16. Bilal, M. et al. Macromolecular agents with antimicrobial potentialities: A drive to combat antimicrobial resistance. *Int. J. Biol. Macromol.* **103**, 554–574 (2017).
17. Matouskova, P., Marova, I., Bokrova, J. & Benesova, P. Effect of encapsulation on antimicrobial activity of herbal extracts with lysozyme. *Food Technol. Biotechnol.* **54** (3), 304–316 (2016).
18. Saqib, S. et al. Organometallic assembling of chitosan-iron oxide nanoparticles with their antifungal evaluation against rhizopus oryzae. *Appl. Organomet. Chem.* **33** (11), e5190 (2019).
19. Saqib, S. et al. Catalytic potential of endophytes facilitates synthesis of biometallic zinc oxide nanoparticles for agricultural application. *BioMetals* **35** (5), 967–985 (2022).
20. Zardini, H. Z., Amiri, A., Shanbedi, M., Maghrebi, M. & Baniadam, M. Enhanced antibacterial activity of amino acids-functionalized multi walled carbon nanotubes by a simple method. *Colloids Surf. B* **92**, 196–202 (2012).
21. Zare-Zardini, H., Amiri, A., Shanbedi, M., Memarpoor-Yazdi, M. & Asoodeh, A. Studying of antifungal activity of functionalized multiwalled carbon nanotubes by microwave-assisted technique. *Surf. Interface Anal.* **45** (3), 751–755 (2013).
22. Zardini, H. Z. et al. Microbial toxicity of ethanolamines—Multiwalled carbon nanotubes. *J. Biomed. Mater. Res. Part A* **102** (6), 1774–1781 (2014).
23. Zare-Zardini, H. et al. Investigating the antimicrobial activity of vancomycin-loaded soy protein nanoparticles. *Interdisc. Perspect. Infect. Dis.* **2022**, (2022).
24. Parsaeian, M. R. et al. Evaluating the biological activities of functionalized magnetic iron oxide nanoparticles with different concentrations of aqueous pine leaves extract. *J. Indian Chem. Soc.* **99** (10), 100707 (2022).
25. Qasim Nasar, M. et al. Seripheidium quettense mediated green synthesis of biogenic silver nanoparticles and their theranostic applications. *Green Chem. Lett. Rev.* **12** (3), 310–322 (2019).
26. Zare-Zardini, H. et al. Design of a new coating agent based on graphene oxide and antimicrobial/spermicidal peptide (sarcotoxin pd) for condom coating: New strategy for prevention of unplanned pregnancy and sexually transmitted infections. *J. Nanomater.* **2023**, (2023).
27. Harish, V. et al. Review on nanoparticles and nanostructured materials: bioimaging, biosensing, drug delivery, tissue engineering, antimicrobial, and agro-food applications. *Nanomaterials* **12** (3), 457 (2022).
28. Chen, L. et al. Recent progress in targeted delivery vectors based on biomimetic nanoparticles. *Signal. Transduct. Target. Therapy* **6** (1), 225 (2021).
29. Hornok, V. Serum albumin nanoparticles: problems and prospects. *Polymers* **13** (21), 3759 (2021).
30. Mirjalili, A. et al. From wild mallow to silver's embrace: A tale of two hydrogels and diabetic wound healing (Chitosan/Polycaprolactone/Polyvinyl Alcohol-Based hydrogel containing Malva sylvestris extract and Chitosan/Polycaprolactone/Polyvinyl Alcohol-based hydrogel containing malva sylvestris extract and silver nanoprticles). *BioNanoScience* **15** (1), 1–14 (2025).
31. Zare-Zardini, H. et al. Slow release curcumin-containing soy protein nanoparticles as anticancer agents for osteosarcoma: synthesis and characterization. *Prog. Biomater.* **11** (3), 311–320 (2022).

32. Yazdi, A. M., Mazidi, M., Tarzi, M. G. & Zardini, H. Z. Investigating the toxicity of germ of date seed on normal and cancerous cell line and P53 gene expression. *Acad. J. Health Sci. Med. Balear.* **38** (3), 62–65 (2023).
33. Zare-Zardini, H. et al. Design of a new coating agent based on graphene oxide and antimicrobial/spermicidal peptide (Sarcotoxin Pd) for condom coating: new strategy for prevention of unplanned pregnancy and sexually transmitted infections. *J. Nanomater.* **2023** (1), 2487468 (2023).
34. Vojdani Nejad Yazdi, S., Zare-Zardini, H., Miresmaeili, M. & Fesahat, F. Evaluating the toxicity of doxorubicin-silk fibroin nanoparticles and its effect on P53 gene expression in breast cancer cell line. *Iran. J. Breast Dis.* **15** (1), 71–86 (2022).
35. Callister, W. D. Jr & Rethwisch, D. G. *Materials Science and Engineering: an Introduction* (Wiley, 2020).
36. Xu, J. et al. Applications and challenges of ultra-small particle size nanoparticles in tumor therapy. *J. Control. Release* **353**, 699–712 (2023).
37. De Jong, W. H. & Borm, P. J. Drug delivery and nanoparticles:applications and hazards. *Int. J. Nanomed.* **3** (2), 133–149 (2008).
38. Naeem, Z., Rana, T. & Javaid, S. Evaluating frontiers in nanotechnology: A review of novel nanoparticle technology in drug delivery systems (DDS). *Currents Pharm. Res.* **1** (1), 16–46 (2023).
39. Deng, M., Rao, J-D., Guo, R., Li, M. & He, Q. Size-adjustable nano-drug delivery systems for enhanced tumor retention and penetration. *Pharm. Fronts* **3** (03), e98–e112 (2021).
40. Joseph, T. M. et al. Nanoparticles: taking a unique position in medicine. *Nanomaterials* **13** (3), 574 (2023).
41. Hadji, H. & Bouchemal, K. Effect of micro-and nanoparticle shape on biological processes. *J. Control. Release* **342**, 93–110 (2022).
42. Mackay, M. E. et al. General strategies for nanoparticle dispersion. *Science* **311** (5768), 1740–1743 (2006).
43. Chapter 3 - Characteristics and behavior of nanoparticles and its dispersion systems. In: Naito M, Yokoyama T, Hosokawa K, Nogi K, editors. *Nanoparticle Technology Handbook (Third Edition)*. 109 – 68. (Elsevier, 2018).
44. Hoshyar, N., Gray, S., Han, H. & Bao, G. The effect of nanoparticle size on in vivo pharmacokinetics and cellular interaction. *Nanomedicine (London England)* **11** (6), 673–692 (2016).
45. He, C., Hu, Y., Yin, L., Tang, C. & Yin, C. Effects of particle size and surface charge on cellular uptake and biodistribution of polymeric nanoparticles. *Biomaterials* **31** (13), 3657–3666 (2010).
46. Augustine, R. et al. Cellular uptake and retention of nanoparticles: insights on particle properties and interaction with cellular components. *Mater. Today Commun.* **25**, 101692 (2020).
47. Hudz, N. & Kobylinska, L. *Mentha piperita*: essential oil and extracts, their biological activities, and perspectives on the development of new medicinal and cosmetic products. **28** (21), (2023).
48. Eftekhari, A. et al. Phytochemical and nutra-pharmaceutical attributes of mentha spp.: A comprehensive review. *Arab. J. Chem.* **14** (5), 103106 (2021).
49. Raeisi, H. et al. Pleiotropic effects of *Mentha longifolia* L. extract on the regulation of genes involved in inflammation and apoptosis induced by clostridioides difficile ribotype 001. *Front. Microbiol.* **14**, 1273094 (2023).
50. Rahimifard, N. et al. Cytotoxic effects of essential oils and extracts of some Mentha species on Vero, Hela and Hep2 cell lines. (2010).
51. Elzoghby, A. O., Samy, W. M. & Elgindy, N. A. Albumin-based nanoparticles as potential controlled release drug delivery systems. *J. Control. Release* **157** (2), 168–182 (2012).
52. Lei, C. et al. Hyaluronic acid and albumin based nanoparticles for drug delivery. *J. Control. Release* **331**, 416–433 (2021).
53. Kunde, S. S. & Wairkar, S. Targeted delivery of albumin nanoparticles for breast cancer: A review. *Colloids Surf. B* **213**, 112422 (2022).
54. Wang, L., Hu, C. & Shao, L. The antimicrobial activity of nanoparticles: present situation and prospects for the future. *Int. J. Nanomed.* **12**, 1227–1249 (2017).
55. Adeyemi, S. B. et al. Polymeric nanoparticles for enhanced delivery and improved bioactivity of essential oils. *Heliyon* **9** (6), e16543 (2023).
56. Faisal, S. et al. Bio synthesis, comprehensive characterization, and multifaceted therapeutic applications of BSA-resveratrol coated platinum nanoparticles. *Sci. Rep.* **14** (1), 7875 (2024).
57. Naikoo, G. A. et al. Bioinspired and green synthesis of nanoparticles from plant extracts with antiviral and antimicrobial properties: A critical review. *J. Saudi Chem. Soc.* **25** (9), 101304 (2021).
58. Kumari, S. & Goyal, A. Bioactive loaded novel nano-formulations for targeted drug delivery and their therapeutic potential. **14** (5), (2022).
59. Swain, S. S., Paidesetty, S. K., Padhy, R. N. & Hussain, T. Nano-technology platforms to increase the antibacterial drug suitability of essential oils: A drug prospective assessment. *OpenNano* **9**, 100115 (2023).
60. Azmi, K., Qrei, W. & Abdeen, Z. Screening of genes encoding adhesion factors and biofilm production in methicillin resistant strains of *Staphylococcus aureus* isolated from palestinian patients. *BMC Genom.* **20** (1), 578 (2019).
61. Tuon, F. F., Suss, P. H., Telles, J. P., Dantas, L. R. & Borges, N. H. Antimicrobial treatment of *Staphylococcus aureus* biofilms. **12** (1), (2023).
62. Ahmad, N. et al. Antimicrobial efficacy of Mentha piperata-derived biogenic zinc oxide nanoparticles against UTI-resistant pathogens. *Sci. Rep.* **13** (1), 14972 (2023).
63. Atta, S. et al. Antibacterial potential and synergistic interaction between natural polyphenolic extracts and synthetic antibiotic on clinical isolates. *Saudi J. Biol. Sci.* **30** (3), 103576 (2023).
64. Khare, T. et al. Exploring phytochemicals for combating antibiotic resistance in microbial pathogens. *Front. Pharmacol.* **12**, 720726 (2021).
65. El-Aziz, A. R. M. A., Al-Othman, M. R., Mahmoud, M. A., Shehata, S. M. & Abdelazim, N. S. Chitosan nanoparticles as a carrier for mentha longifolia extract: synthesis, characterization and antifungal activity. *Curr. Sci.* 2116–2122. (2018).
66. Kumar, P., Mishra, S., Malik, A. & Satya, S. Preparation and characterization of PEG-mentha oil nanoparticles for housefly control. *Colloids Surf. B* **116**, 707–713 (2014).
67. Ashrafi, B. et al. Mentha Piperita essential oils loaded in a chitosan nanogel with inhibitory effect on biofilm formation against S. mutans on the dental surface. *Carbohydr. Polym.* **212**, 142–149 (2019).
68. Muntean, D. et al. Evaluation of essential oil obtained from mentha×piperita L. against multidrug-resistant strains. *Infect. Drug Resist.* **12**, 2905–2914 (2019).
69. Laein, S. S. & Khanzadi, S. Peppermint essential oil-loaded solid lipid nanoparticle in gelatin coating: characterization and antibacterial activity against foodborne pathogen inoculated on rainbow trout (Oncorhynchus mykiss) fillet during refrigerated storage. **87** (7), 2920–2931. (2022).
70. Romero-Montero, A. & Melgoza-Ramírez, L. J. Essential-oils-loaded biopolymeric nanoparticles as strategies for microbial and biofilm control. *Curr. Status* **25** (1), (2023).
71. Gao, W., Chen, Y., Zhang, Y., Zhang, Q. & Zhang, L. Nanoparticle-based local antimicrobial drug delivery. *Adv. Drug Deliv. Rev.* **127**, 46–57 (2018).
72. Razei, A. et al. Nano and microparticle drug delivery systems for the treatment of Brucella infections. *Biomed. Pharmacother.* **169**, 115875 (2023).
73. Gao, W., Thamphiwatana, S., Angsantikul, P. & Zhang, L. Nanoparticle approaches against bacterial infections. *Wiley Interdisc. Rev. Nanomed. Nanobiotechnol.* **6** (6), 532–547 (2014).
74. Huang, Y. et al. Nanotechnology's frontier in combatting infectious and inflammatory diseases: prevention and treatment. *Signal. Transduct. Target. Therapy* **9** (1), 34 (2024).

15

Author contributions

In this study, all authors contributed to the design, writing, and review of the manuscript. HZZ managed and supervised the project as well as data collection. AA managed and supervised the project and contributed to data collection and manuscript revision. ES contributed to Data collection and particle synthesis. AJ1 contributed to particle synthesis. AJ2 contributed to search and data collection and biological assay. AP contributed to data analysis. JJ contributed to search and data collection and editions of manuscript. STH contributed to experimental section. MAH contributed to particle synthesis and characterization. NS contributed to experimental section.

Declarations

Competing interests

The authors declare no competing interests.

Additional information

Correspondence and requests for materials should be addressed to H.Z.-Z., A.A. or A.J.

Reprints and permissions information is available at www.nature.com/reprints.

Publisher's note Springer Nature remains neutral with regard to jurisdictional claims in published maps and institutional affiliations.